Quantum efficiency measurements of eROSITA pnCCDs

Stefanie Ebermayer[a], Robert Andritschke[a], Johannes Elbs[a], Norbert Meidinger[a], Lothar Strüder[a], Robert Hartmann[a,b], Alexander Gottwald[c], Michael Krumrey[c] and Frank Scholze[c]

[a]MPI Semiconductor Laboratory, Otto-Hahn-Ring 6, 81739 Munich, Germany;
[b]PNSensor GmbH, Römerstr. 28, 80803 Munich, Germany;
[c]Physikalisch-Technische Bundesanstalt (PTB), Abbestr. 2-12, 10587 Berlin, Germany

ABSTRACT

For the eROSITA X-ray telescope, which is planned to be launched in 2012, detectors were developed and fabricated at the MPI Semiconductor Laboratory. The fully depleted, back-illuminated pnCCDs have an ultrathin pn-junction to improve the low-energy X-ray response function and quantum efficiency. The device thickness of 450 μm is fully sensitive to X-ray photons yielding high quantum efficiency of more than 90% at photon energies of 10 keV. An on-chip filter is deposited on top of the entrance window to suppress visible and UV light which would interfere with the X-ray observations. The pnCCD type developed for the eROSITA telescope was characterized in terms of quantum efficiency and spectral response function. The described measurements were performed in 2009 at the synchrotron radiation sources BESSY II and MLS as cooperation between the MPI Semiconductor Laboratory and the Physikalisch-Technische Bundesanstalt (PTB). Quantum efficiency measurements over a wide range of photon energies from 3 eV to 11 keV as well as spectral response measurements are presented. For X-ray energies from 3 keV to 10 keV the quantum efficiency of the CCD including on-chip filter is shown to be above 90% with an attenuation of visible light of more than five orders of magnitude. A detector response model is described and compared to the measurements.

Keywords: pnCCD, eROSITA, quantum efficiency, detector response, entrance window

1. INTRODUCTION

1.1 Motivation

Semiconductor detectors for X-rays have been successfully used in the past in numerous astronomical research projects. Based on the technology of the detectors for the XMM-Newton mission, pnCCDs were developed for the eROSITA (extended Roentgen Survey with an Imaging Telecope Array) instrument.[1] One part of this mission is an imaging all-sky survey for X-rays in the energy range of 200 eV to 10 keV with high spectral and angular resolution. An essential prerequisite for the all-sky survey is the suppression of visible and UV light. It has to be blocked from the detector to avoid shifting or broadening of measured X-ray lines. According to the eROSITA mission requirements, visible light suppression should be more than 10^5. To achieve high quantum efficiency (QE) in the X-ray range while minimizing the incidence of optical and UV light, a compromise in layer thickness and material composition has to be chosen. The choice of materials depends on absorption properties in different energy regimes as well as technological aspects.
One of two possible entrance windows for the eROSITA detector is a combination of silicon dioxide, silicon nitride and aluminium. This filter was manufactured as on-chip solution and therefore permits to avoid the use of carbon which is usually contained in external filters. The typical discontinuity in quantum efficiency at the carbon absorption edge at 284 eV can thus be prevented. In fact, the aluminium layer reduces the QE at low X-ray energies, but the spectral resolution is not affected. On-chip filters do not involve the risk of rupture during launch like external filters, which can in worst case lead to lethal damage to the camera. There has never been an astronomical X-ray survey with a carbon-free entrance window before which opens opportunities for high-accuracy measurements at this energy with eROSITA. pnCCDs with a second possible entrance window configuration have also been manufactured at the Semiconductor Laboratory. These detectors have no on-chip

Further author information: (Send correspondence to S. Ebermayer)
S. Ebermayer: E-mail: sce@hll.mpg.de

aluminium coating and could thus only be operated with an additional external blocking filter. This kind of filter could be made of a supporting organic foil with additional aluminium and tin films such as used for the XMM-Newton focal-plane cameras. A carbon absorption edge in the quantum efficiency results from this solution, while the blocking properties in the XUV (extreme ultra-violet) range are improved compared to the first option.
The following measurements were performed with detectors of the first of the described entrance window configurations. The goal was to confirm existing calculations about quantum efficiency and to serve as a first step towards detector calibration. Additionally, these measurements contribute to the full understanding of photon and electron interaction processes inside the entrance window that are responsible for the spectral response function. This knowledge is crucial to analyse detector data correctly and to improve entrance window development. The measurements were performed with a pnCCD of the eROSITA production. By using a pnCCD we were able to connect the measured spectral response function and quantum efficiency as the same device could be used for both measurements. Additionally, spectral responsivity measurements were done with a diode of the same material and entrance window to analyse the absorption edge fine-structure with a high resolution and high relative accuracy.

1.2 The pnCCD detector

The pnCCD is a 3-phase, back-illuminated charge coupled device with fully depleted chip thickness of 450 μm. The transfer registers and the photon entrance window are realized by boron implantations in ultra-pure n-type silicon. The charge is transferred in a depth of about 7 μm below the front side. The detector is divided in two parts, namely image area and frame store area. When the pnCCD is operated in frame store mode, the image is transferred from image to frame store area by a fast transfer. Then it is read out row by row from the frame store area while photons are again accumulated in the image area for the next picture. In fullframe mode both pnCCD parts are used as sensitive area and the pixels are transferred and read out row by row. The pnCCD developed for the eROSITA mission[1] has 384 transfer channels with each 384 pixels in the image and frame store area. The pixel size is 75 μm$\times$ 75 μm in the image area and 51 μm$\times$ 75 μm in the frame store area. All channels are equipped with an anode which is connencted to the gate of a monolithically integrated JFET. A bond wire connects the source of each of the transistors to the input of a signal processor channel of the CAMEX.[2] The CAMEX (CMOS Amplifier and MultiplEXer) ASIC allows amplification and shaping of signals in 128 channels in parallel. Therefore, three CAMEX chips are necessary for the read-out of one eROSITA pnCCD.
The detector used for the described measurements is of the eROSITA production and only differs from the flight pnCCDs in its size. The number of channels is 128 instead of 384 as well as the number of pixels in image and frame store area.

2. MEASUREMENT SETUP

2.1 Measurement facilities

Measurements were conducted in the PTB laboratories at the synchrotron radiation facilites BESSY II and Metrology Light Source (MLS) in Berlin. For X-ray measurements, low intensity was achieved by running the experiment during single bunch mode at BESSY II and by using slits to lower the photon flux. The storage ring current at the MLS was adjusted to our experiment.

- Normal-incidence Monochromator for the ultraviolet (UV) and vacuum-ultraviolet (VUV) spectral range at the MLS: The metrology light source is a low-energy storage ring that offers the possibility of high precision measurements in the spectral range from the far infrared/THz to the extreme ultraviolet (EUV) region.[3] Measurements were performed at the normal incidence monochromator in the spectral range from 2.8 eV to 35 eV. The illuminated area amounted 2 mm $\times$ 5 mm.
- Grazing incidence Monochromator at BESSY II: The plane grating monochromator beamline[4] of SX700 type at BESSY II was used for VUV (vacuum ultra-violet) and X-ray energies from 40 eV to 1700 eV. The illuminated spot was around 0.5 mm $\times$ 2 mm to 2 mm $\times$ 4 mm. The radiation is highly monochromatic in terms of energy resolution. For photon energies above 600 eV the fraction of straylight and high-order light increases with energy especially if the beam is strongly attenuated by slits.

- Four-Crystal Monochromator at BESSY II: Measurements at energies from 1800 eV to 11 keV were performed at the four-crystal-monochromator beamline. At this beamline, the spectral resolving power ranges between 4000 and 12000, the higher order contribution decreases from 10^{-3} to 10^{-8} with increasing photon energy.[5] The illuminated spotsize was around 1 mm $\times$ 2 mm large.

2.2 Measurement details

The data for evaluation of the spectral response function was taken at very low intensity of around 5 to 20 photons per frame with an illuminated area of 100 to 3000 pixels on the CCD. In the measured spectra the pileup peak was clearly separated from the main peak, while a minimum statistic of 100.000 photons per measurement was accumulated.
The quantum efficiency measurements with the pnCCD were performed for approximately 200 different photon energies. A measurement set consisted of a PTB reference diode measurement and a pnCCD measurement. The quantum efficiency was determined from the integrated intensity of the illuminated spot. For a measurement with single photon counting, the reference current at the PTB-diode would have been too low to achieve acceptable accuracy. The responsivity of the PTB reference has an uncertainty of 1%. For each dataset, the energy was set at the monochromator and intensity was adjusted in a way that the generated charge per CCD channel did not exceed the limit for linear amplification and the reference diode current was at minimum 1 pA. For very low reference currents, a current measurement was performed several times with dark current values taken before and after the signal current to increase accuracy. The reference diode was then removed from the beam to illuminate the CCD for about one minute. Throughout the measurement, the ring current was logged to be able to correct both CCD and reference diode data as the synchrotron radiation reduces with time. The detector was operated in frame store mode (normal operating mode) with a cycle time of 5 ms for almost all measurements. Above 2.5 keV, fullframe mode was used at high frame rates, so that the picture was smeared over the whole detector channel length. This avoids pixel intensities above the maximum readout range. Additional measurements were done to verify the gain linearity by changing cycle time, operation mode (fullframe and frame store) and intensity. Thereby the measured intensity per channel, pixel and frame could be varied separately. No saturation effects or non-linearity effects were observed when comparing the different measurement methods. For the VUV measurements around 10 eV, where the attenuation reaches more then 10^8, cycle time had to be raised up to 1 s to get a measurable signal on the detector.
The monochromator energy resolution allowed to measure in energy steps of down to 1 eV to resolve the fine-structure of absorption edges. Charge integration in comparison to single photon counting could be performed in shorter time and allowed to accumulate 200 datapoints at different energies. The CCD temperature was held constant throughout the measurement at $(-79 \pm 1)^\circ$C. At this temperature stability the detector gain can be treated as constant.
The spectral responsivity measurements with a pn-diode of eROSITA wafers (further called MPI-diode) were performed at energies between 35 eV and 1800 eV. The current at the PTB reference diode (PTB-diode) for this measurement was in the order of μA which leads to a higher accuracy regarding the current measurement. The MPI-diode was cooled by a Peltier element and reached a temperature of around -10°C. The depletion voltage at the MPI diode was 30 V which is significantly lower than the depletion voltage of the pnCCD. However, this would only affect photon absorption at high penetration depths for energies above 4 keV while the MPI diode was only used for measurements up to 1.8 keV.

3. BLOCKING FILTER PROPERTIES

In order to fully characterize the attenuation of visible light and UV radiation of the filter, spectral responsivity measurements for photon energies from 2.8 eV up to 100 eV were conducted with the pnCCD. The integrated signal per frame on the pnCCD and the signal on the PTB reference diode were measured for each photon energy. The fractional amount of incident photons to measured photons defines the attenuation factor. Values for the eletron-hole pair creation energy were taken from Scholze[6] and Hartmann.[7] Special attention had to be drawn to higher diffraction order radiation from the monochromator. Although it can be suppressed down to a fraction at maximum 0.15%, the QE discontinuity at 10 eV leads to an enhancement of higher photon energies of up to 10^5 and hinders the measurements in this energy range. Different solid state filters (MgF_2, LiF, quartz) were used behind the monochromator to block higher monochromator orders. Preliminary measurements to confirm visible

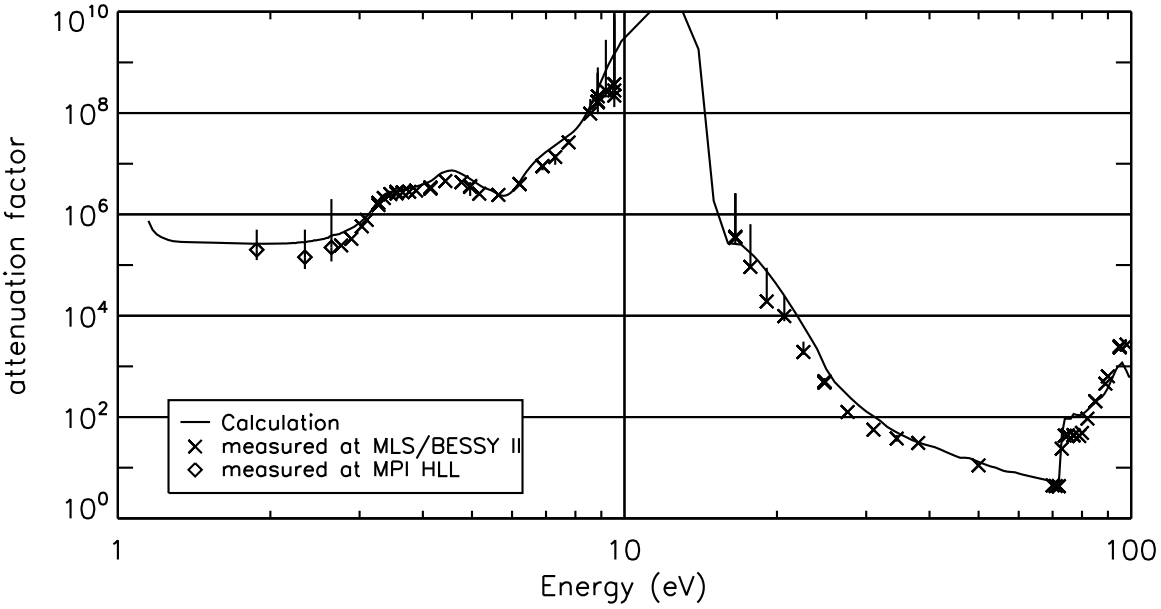

Figure 1. Attenuation factor in the blocking range of the eROSITA entrance window. The line represents a calculation including photon absorption in all layers and taking into account the thin film structure of the aluminium layer. Measurements at MLS/BESSY II and at the Semiconductor Laboratory (MPI HLL) are displayed.

light attenuation have been conducted at the semiconducor laboratory by illuminating pnCCDs and diodes with LEDs and Lasers. Fig. 1 shows these results together with the measurement data taken at MLS/BESSY II . The calculation for optical and UV attenuation takes into account the thin film structure of the aluminium layer and deviates strongly from calculations for bulk aluminium absorption data. Attenuation of more than 10^5 is reached for optical light and UV radiation up to almost 20 eV. Between 20 eV and 70 eV the aluminium gets less absorbing and leads to a minimum attenuation at energies around 70 eV. The increase of attenuation at 72 eV is due to the aluminium L-edge (see table 1). For energies from 10 eV to 15 eV there was no accurate measurement possible as the attenuation factor is very high and decreases with energy. This results in an extremely low signal at the detector while high-order radiation from the monochromator passes the blocking filter to a high amount. The error bars in Fig. 1 are mainly dominated by the effect of high-order radiation which is assumed to be 0.15%. The deviation between measured and calculated values for energies above 15 eV can furthermore be explained by the accuracy of the used absorption data, as for this photon energy range the variation between different literature data sources[8,9] for absorption coefficients is significant.

4. X-RAY QUANTUM EFFICIENCY

4.1 Overview

In this work the term quantum efficiency will be defined as follows: the total QE describes the ratio of detected events compared to the number of photons hitting the detector. Events are counted even if their energy in the spectrum is different to the original photon energy. The full peak QE only refers to those events that are measured at an energy range of $\pm 2 \cdot \mathrm{FWHM}$ (full width half maximum) around the main peak. It is therefore slightly lower than the total quantum efficiency.

4.2 Model description

The model describing the quantum efficiency contains the following mechanisms: (a) At the outer part of the entrance window, photons are absorbed according to Beers law (see Eq. 1). The intensity I of photons passing a material depends on the absorption length λ_{abs} and the material thickness d. As a result, a fraction of photons

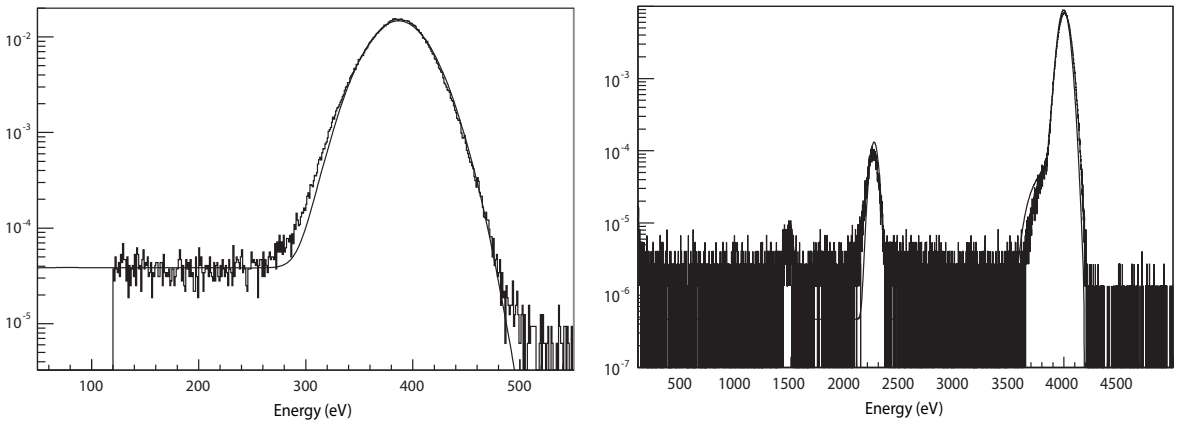

(a) E_{photon} = 396 eV: the low-energy shelf is caused by photoelectrons created in the silicon dioxide

(b) E_{photon} = 4000 eV: besides the main peak there is an Al fluorescence peak at 1486 eV and a Si escape peak at 2260 eV

Figure 2. Measured spectra and theoretical model of the spectral response function.

is absorbed in the outer layers and is therefore lost for the detector. As a first approximation, this effect already describes the quantum effiency quite well. All further described effects have additional but smaller influence.

$$I(d) = I_0 \cdot \exp(-\frac{d}{\lambda_{abs}}) \tag{1}$$

(b) Photoelectrons generated by absorption in the silicon dioxide layer can propagate to the silicon. These electrons are subject to energy losses due to scattering and form a low-energy flat shelf in the spectrum between zero and their original energy. The thickness of the oxide layer that contributes to this flat shelf is limited by the maximum pathlength of electrons. We used the formula by Fitting[10] to define the relevant oxide layer thickness depending on photon energy. This part of the oxide layer is not included in the absorption calculation of Eq. 1. The third mechanism (c) involves partial charge losses at the boundary layer between SiO_2 and Si. In the spectrum, this leads to a shoulder at the low energy part of the main peak. The effects of (b) and (c) were modeled by fitting spectra with the partial event model (see Popp[11]) with the relevant oxide thickness. As further contribution (d) to quantum efficiency, the silicon escape peak is taken into account. Si-K fluorescence photons that leave the detector form a peak at energies shifted by 1739 eV to the original photon energy. When regarding the full-peak QE these photons do not contribute. For the spectral response model, the intensity of the silicon escape peak was calculated by Reed's[12] formula. (e) For high X-ray energies ($>$ 8 keV), detector thickness affects the quantum efficiency. This is accounted for by the absorption of photons in 450 μm silicon. The effect of the aluminium fluorescence peak to quantum efficiency can be neglected.

Finally, the quantum efficiency calculation can be divided into two steps: the number of total events in the spectrum can be calculated out of the mechanisms described in (a) and (e). The spectral response function, which is affected by (b), (c) and (d) leads to a factor $f_{fullpeak}$ to determine the fractional amount of events that contribute to the full peak quantum efficiency. This factor is in the range between 0.96 and 0.99 as displayed in Fig. 4.

Figure 2 gives an overview about the spectral response of the eROSITA detector. Even though there are still small deviations from the model, the agreement between measurement and theoretical description of the spectral response is sufficient to use the theoretical spectral response function for quantum efficiency calculations (see section 4.3). The uncertainty in peak position was added to the error contributions in QE evaluation. Further details on spectral response functions of semiconductor detectors can be found in Eggert[13] and Scholze.[14,15]

For the calculation of photon absorption according to Eq. 1 data from several sources was used. Tabulated data were available in Henke et al.,[9,16] Palik[8,17,18] and Owens et al.[19] At the oxygen-K, nitrogen-K and aluminium-K absorption edges, the available data were expanded by interpolating from the measurements (see section 4.4). The layer thicknesses of SiO_2 and Si_3N_4 were measured at the Semiconductor Laboratory. The deviation from

the nominal thickness throughout the wafer is less than 1%. The aluminium thickness is known to an accuracy of around 5%. The calculated QE curve in Fig. 3 represents the best fit to the measured QE data with aluminium layer thickness as free parameter. The aluminium layer thickness that fits our measured QE data is within the expected range.

4.3 QE measurement results

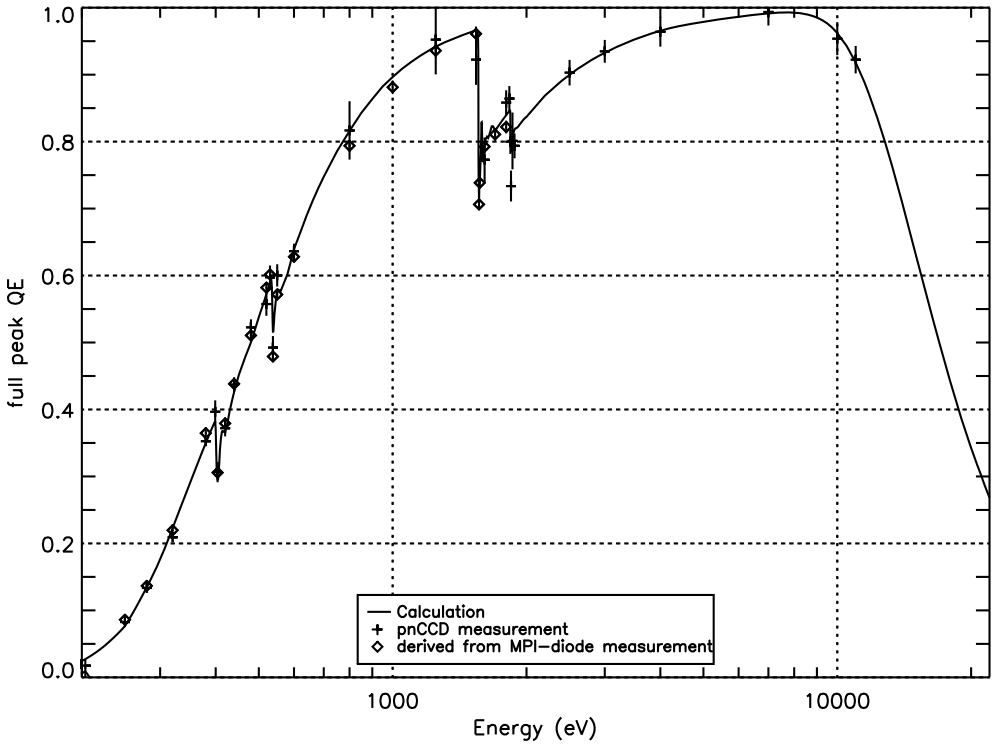

Figure 3. Full peak quantum efficiency in the energy range of interest for the eROSITA mission. For better visibility not all measured data points around the absorption edges are displayed.

For evaluation of the quantum efficiency measurements, the number of events per second measured with the pnCCD $n_{measured}$ was extracted from the integrated signal over the illuminated spot I_{CCD} in adu (arbitrary digital units) per frame as described in Eq. 2. A shift of the mean event energy E_{mean} due to oxide shelf events and silicon escape events was considered. For better understanding, units are given in round brackets in the following equations.

$$n_{measured} = \frac{I_{CCD}(adu)}{gain_{CCD}(adu \cdot eV^{-1}) \cdot E_{mean}(eV) \cdot t_{frame}(s)} \tag{2}$$

The pair creation energy (eV/electron) and the amplification factor (adu/electron) is assumed to be constant and leads to a constant gain in adu per eV. The number of photons n_{in} incident on the detector entrance window was determined according to Eq. 3 out of the PTB reference current and the responsivity of the PTB diode R_{PTB}.

$$n_{in} = \frac{I_{PTB}(A)}{R_{PTB}(A \cdot W^{-1}) \cdot E_{ph}(J)} \tag{3}$$

The total quantum efficiency can then be calculated as the fraction of detected photons to incident photons (see Eq. 4) normalized to the ring currents $I_{Ring,PTB}$ and $I_{Ring,MPI}$ during measurement. To calculate the full-peak quantum efficiency, a correction factor $f_{fullpeak}$ was determined from the spectral response model described in section 4.2. This correction factor (see Fig. 4) describes the fraction of counted events compared to the total number of events in the integrated spectral response function.

$$QE_{fullpeak} = \frac{n_{measured}(s^{-1})}{n_{in}(s^{-1})} \cdot \frac{I_{Ring,PTB}(A)}{I_{Ring,CCD}(A)} \cdot f_{fullpeak} \tag{4}$$

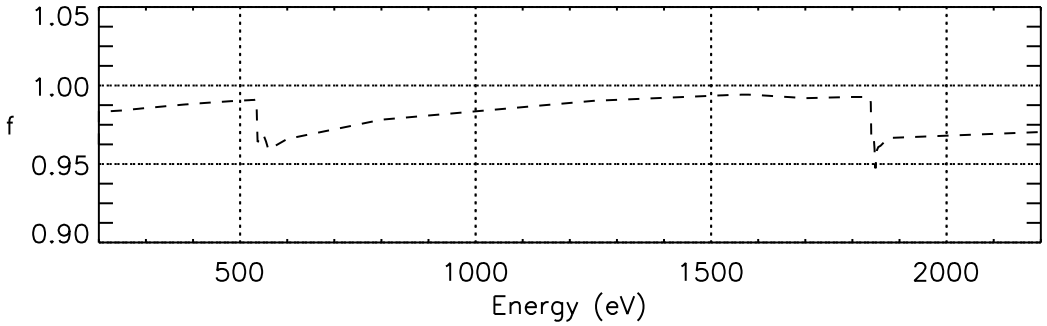

Figure 4. Fraction $f_{fullpeak}$ of events that are counted for the full peak QE out of all events in the measured spectrum. Below the Si-K edge, $f_{fullpeak}$ is mainly influenced by the low energy shelf, while above the Si-K edge the silicon escape peak is the dominant influence.

The measured full peak QE of the pnCCD with eROSITA entrance window is shown in Fig. 3. At energies between 600 eV and 1800 eV high-order radiation from the monochromator rose up to several percent whenever the beam was attenuated strongly by slits. This effect could be seen from the spectral measurements with the pnCCD and was corrected in evaluation by considering the nominal and first higher order photon energy. Instabilities in slit positions lead to increased statistical error for energies around the Al-K edge as the slit width was extremely small. Both effects increase the estimated measurement uncertainty for pnCCD measurements at the mentioned photon energies as shown in Fig. 3.

4.4 Absorption Edges

Shell Element	*K 1s*	*L1 2s*	*L2 2p1/2*	*L3 2p3/2*
7 N	409.9	37.3		
8 O	543.1	41.6		
13 Al	1559.6	117.8	72.95	72.55
14 Si	1839	149.7	99.82	99.42

Table 1. Electron binding energies (in eV).[20]

The absorption edges observed in the quantum effiency curve are caused by discontinuities in the absorption coefficients of the entrance window materials. They occur whenever the photon energy corresponds to the binding energy of electrons. Table 1 shows electron binding energies taken from Thompson[20] for N, O, Al and Si in their natural forms. In compounds like Si_3N_4 those edges can be shifted in respect to the given values because of the change in electron binding energy. Prigozhin[21] has already presented measurements about the absorption edges in the QE of X-ray CCDs for Si_3N_4 and SiO_2. In our measurement results, the edge energies are 537 eV for oxygen-K in SiO_2 and 401 eV for nitrogen-K in Si_3N_4, which matches Prigozhins results. The aluminium-K edge was found at 1559 eV as expected. The silicon K-edge is expected to split into two parts,[21] at an energy of 1847 eV due to the SiO_2 and 1845 eV due to Si_3N_4. In the range of measurement accuracy, results match these expectations, while the detailed structure of this absorption edge cannot be resolved. Additional oscillatory fine structure can be seen in a range of up to 20 eV to 200 eV above the absorption edges (see fig. 5). In this regime, the absorption probability is modulated with energy due to the chemical or physical state of the atoms. X-ray Absorption Near Edge Structure (XANES) extends up to some hundred eV above an absorption edge

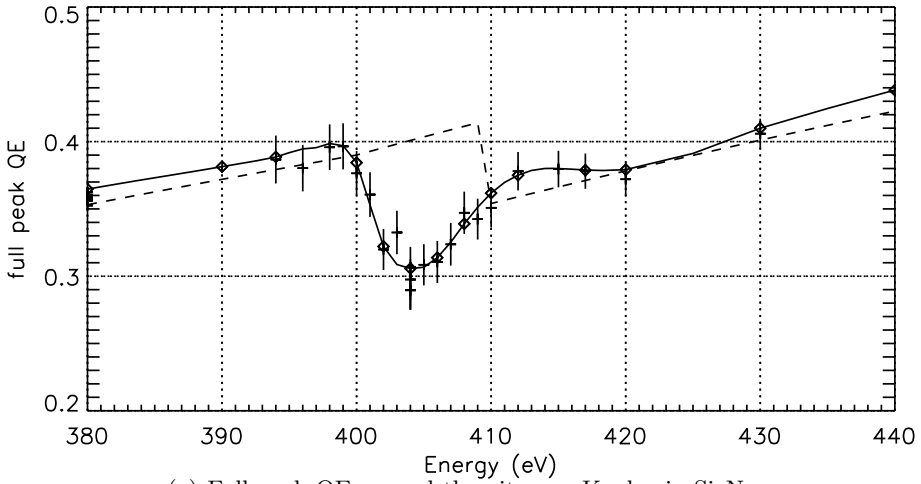

(a) Full peak QE around the nitrogen-K edge in Si_3N_4

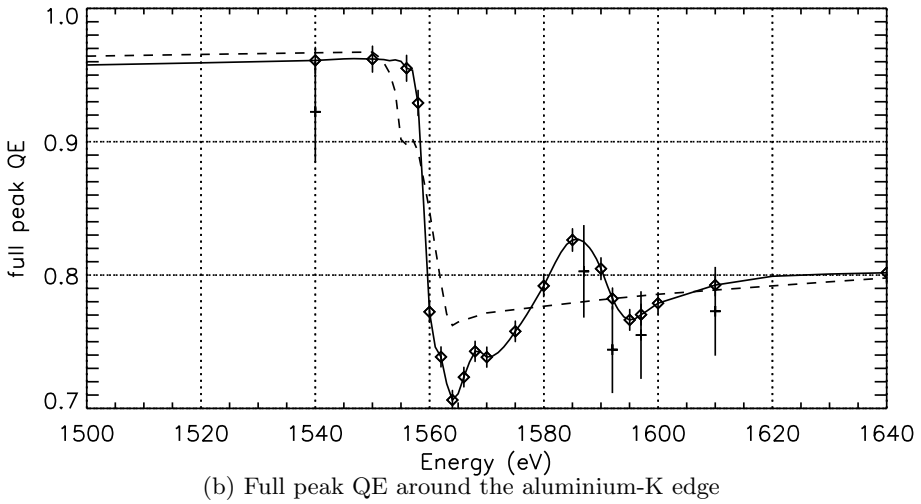

(b) Full peak QE around the aluminium-K edge

Figure 5. Full Peak QE at the absorption edges. Crosses mark pnCCD measurement data, diamonds represent data derived from MPI-diode measurements which were used to extract absorption data. The dashed line shows the QE calculation using literature data which does not take into account fine-structure or edge-shift in chemical compounds. The solid line connects MPI-diode measurement values as a guide to the eye.

and originates in constructive and destructive interference of photoelectrons backscattered from the atom lattice. Extended X-ray Absorption Fine Structure (EXAFS) describes oscillations very close (up to 30 eV) to the absorption edge and is mainly influenced by oxidation state and coordination chemistry (e.g. cubic, tetrahedral) of the atoms.[22]

Figure 5 shows the full peak quantum efficiency around the N-K and Al-K absorption edges. The dashed line shows the calculation based on tabulated absorption data as described in section 4.2. This data does not take into account the edge energy shift in compounds or any absorption fine structure. Absorption coefficients have therefore be extracted from our quantum efficiency measurement. For this purpose, the deviation between measurement data and literature data at energy values sufficiently far away from the absorption edges was determined and was superimposed as linear slope on the measurement data. Then the absorption coefficient could be determined and interpolated out of the measurement data. Thereby a steady transition between interpolated data and the literature data is achieved. The purpose of this data extraction is to get the best possible absorption data for the materials used in the eROSITA entrance window.

5. SUMMARY AND OUTLOOK

We have performed extensive measurements of the detector response with a pnCCD of the eROSITA type over a wide photon energy range. Radiation attenuation of photons with energies from 2.8 eV to 100 eV was determined. The attenuation reaches more than 10^5 for visible light to VUV radiation. Furthermore, the X-ray quantum efficiency was measured for energies from 100 eV to 11 keV including the absorption edge fine structures. A theoretical model that allows to reproduce the measurement data was described. It was refined by the extraction of absorption data around the oxygen, nitrogen and aluminium K-edges.
Additional to measurements at the monochromators, an experiment with undispersed synchrotron radiation was performed at BESSY II and will be analyzed as a next step. It will expand the existing measurement data and allow to analyse the homogeneity of the QE over the detector area.

ACKNOWLEDGMENTS

The authors wish to thank all semiconductor laboratory and PTB colleagues who supported the preparation, accomplishment and analysis of the experiments.

REFERENCES

1. Meidinger, N., Andritschke, R., Ebermayer, S., Elbs, J., Hälker, O., Hartmann, R., Herrmann, S., Kimmel, N., Predehl, P., Schächner, G., Soltau, H., Strüder, L., and Tiedemann, L., "CCD detectors for spectroscopy and imaging of x-rays with the eROSITA space telescope," in [*SPIE Proceedings Vol. 7435*], (2009).
2. Herrmann, S., Buttler, W., Hartmann, R., Meidinger, N., Porro, M., and Strüder, L., "CAMEX readout ASICs for pnCCDs," in [*IEEE Nuclear Science Symposium Conference Record*], (2008).
3. Brandt, G., Eden, J., Fliegauf, R., Gottwald, A., Hoehl, A., Klein, R., Müller, R., Richter, M., Scholze, F., Thornagel, R., Ulm, G., Bürkmann, K., Rahn, J., and Wüstefeld, G., "The Metrology Light Source - The new dedicated electron storage ring of PTB," *Nuclear Instruments and Methods in Physics Research Section B: Beam Interactions with Materials and Atoms* **258**, 445–452 (May 2007).
4. Scholze, F., T Mmler, J., and Ulm, G., "High-accuracy radiometry in the EUV range at the PTB soft x-ray beamline," *Metrologia* **40**, 224–+ (Feb. 2003).
5. Krumrey, M. and Ulm, G., "High-accuracy detector calibration at the PTB four-crystal monochromator beamline," *Nuclear Instruments and Methods in Physics Research Section A: Accelerators, Spectrometers, Detectors and Associated Equipment* **467-468**, 1175–1178 (July 2001).
6. Scholze, F., Henneken, H., Kuschnerus, P., Rabus, H., Richter, M., and Ulm, G., "Determination of the electron-hole pair creation energy for semiconductors from the spectral responsivity of photodiodes," *Nuclear Instruments and Methods in Physics Research Section A: Accelerators, Spectrometers, Detectors and Associated Equipment* **439**, 208–215 (Jan. 2000).
7. Hartmann, R., Stephan, K. H., and L., S., "The quantum efficiency of pn-detectors from the near infrared to the soft X-ray region," *Nuclear Instruments and Methods in Physics Research Section A: Accelerators, Spectrometers, Detectors and Associated Equipment* **439**, 216–220 (Jan. 2000).
8. Palik, E. D., [*Handbook of Optical Constants of Solids I*], Academic Press (1985).
9. Henke, B., Gullikson, E., and Davis, J., "X-ray interactions: photoabsorption, scattering, transmission, and reflection at E= 50-30000 eV, Z= 1-92," *Atomic data and nuclear data tables* **54**(2), 181–342 (1993).
10. Fitting, H.-J., "Transmission, energy distribution, and SE excitation of fast electrons in thin solid films," *Physica Status Solidi (a)* **26**(2), 525–535 (1974).
11. Popp, M., *Untersuchung und analytische Modellierung der Systemantwort von pn-CCD Detektoren.*, PhD thesis, Ludwig-Maximilians-Universität München (2000).
12. Reed, S. J. B. and Ware, N. G., "Escape peaks and internal fluorescence in x-ray spectra recorded with lithium drifted silicon detectors," *Journal of Physics E: Scientific Instruments* **5**(6), 582– (1972).
13. Eggert, T., *Die Spektrale Antwort von Silizium-Röntgendetektoren*, PhD thesis, Technische Universität München (2004).
14. Scholze, F. and Procop, M., "Modelling the response function of energy dispersive X-ray spectrometers with silicon detectors," *X-Ray Spectrometry* **38**(4), 312–321 (2009).

15. Scholze, F. and Procop, M., "Measurement of detection efficiency and response functions for an si(li) x-ray spectrometer in the range 0.1-5 kev," *X-Ray Spectrometry* **30**(2), 69–76 (2001).
16. Henke, B. L., Lee, P., Tanaka, T. J., Shimabukuro, R. L., and Fujikawa, B. K., "Low-energy x-ray interaction coefficients: Photoabsorption, scattering, and reflection : E = 100-2000 eV Z = 1-94," *Atomic Data and Nuclear Data Tables* **27**, 1–144 (Jan. 1982).
17. Palik, E. D., [*Handbook of Optical Constants of Solids II*], Academic Press (1991).
18. Palik, E. D., [*Handbook of Optical Constants of Solids III*], Academic Press (1997).
19. Owens, A., Fraser, G. W., and Gurman, S. J., "Near K-edge linear attenuation coefficients for Si, SiO2 and Si3N4," *Radiation Physics and Chemistry* **65**, 109–121 (Sept. 2002).
20. Thompson, A. C., Attwood, D. T., Gullikson, E. M., Howells, M. R., Kortright, J. B., Robinson, A. L., and Underwood, J. H., "X-Ray Data Booklet," Lawrence Berkeley National Laboratory University of California Berkeley, California 94720 (2001).
21. Prigozhin, G. Y., Woo, J., Gregory, J. A., Loomis, A. H., Bautz, M. W., Ricker, G. R., and Kraft, S., "X-ray absorption near edge structure in the quantum efficiency of x-ray charge-coupled devices," *Opt. Eng.* **37**, 2848–2854 (Oct. 1998).
22. Lifshin, E., [*X-ray Characterization of Materials*], Wiley-VCH (1999).